Catalysis Today 289 (2017) 29–37

Contents lists available at ScienceDirect

Catalysis Today

journal homepage: www.elsevier.com/locate/cattod

Kinetic study of the ethyl lactate synthesis from triose sugars on Sn/Al_2O_3 catalysts

E. Pighin, V.K. Díez, J.I. Di Cosimo *

Catalysis Science and Engineering Research Group (GICIC), INCAPE, UNL-CONICET, CCT CONICET Santa Fe, Colectora Ruta Nac. 168, km 0, Paraje "El Pozo", 3000 Santa Fe, Argentina

ARTICLE INFO

Article history:
Received 13 April 2016
Received in revised form 9 September 2016
Accepted 3 October 2016
Available online 20 October 2016

Keywords:
Ethyl lactate
Dihydroxyacetone
Ethanol
Lewis acid
Sugars
Kinetic model

ABSTRACT

The reaction kinetics of the liquid-phase synthesis of ethyl lactate from dihydroxyacetone and ethanol was studied on Sn-promoted alumina catalysts. Yields of ≈70% were obtained at 353 K after 7 h of reaction. The effect of the catalyst Sn loading (1–8 wt.%) and reaction temperature (343–373 K) on the reaction kinetics was investigated. The reaction is promoted by Lewis acid sites provided by surface Sn species. A kinetic model based on a pseudohomogeneous mechanism was postulated to describe the reaction network comprising a sequence of consecutive and parallel reaction steps. The kinetic rate constant associated to ethyl lactate formation increases with the number of Lewis acid sites confirming that surface Sn species participate in the kinetically relevant reaction steps. Catalysts were prepared by impregnation and characterized by N_2 physisorption, X-ray diffraction, UV-vis-DRS, FTIR of pyridine and TPD of NH_3.

1. Introduction

Alkyl lactates, the alkyl esters of lactic acid, are platform chemicals that can be obtained from renewable resources, in particular from cellulose residues, sugars and glycerol [1]. Recently, these compounds have attracted much attention because they are high boiling point liquids used as solvents and plasticizers for cellulose plastics and vinyl resins. They have many other applications such as in pharmaceutical, cosmetic and herbicidal formulations [2]. In particular, ethyl lactate (EL) is widely used as a green solvent to replace chlorinated hydrocarbons [3]. It presents environmental, technological and economic advantages for many industrial applications. It is biodegradable, harmless, recyclable and non-corrosive [4].

Alkyl lactates are currently produced from lactic acid and alcohols (methanol, ethanol, butanol), whereas the main method for production of lactic acid is sugar fermentation. The synthesis of alkyl lactates is catalytically promoted by mineral acids, with the consequent technological and environmental hazard. However, several works found in the literature report the synthesis by heterogeneous catalysis using Amberlyst 15, Dowex 50W and heteropolyacids, but the process is equilibrium-limited reaching conversions of just 35% [5–7]. Thus, new routes that explore the upgrading of biomass byproducts or residues without thermodynamic limitations present high technological and economic interest.

In the last decade, many works describe the synthesis of alkyl lactates through a different route from triose sugars and short chain alcohols using acid catalysts. Trioses such as dihydroxyacetone (DHA) and glyceraldehyde (GLA) can be obtained in a biorefinery either by cellulose hydrolysis followed by isomerization and retro-aldol reactions or by oxidation of glycerol [8], the latter being the main byproduct of the biodiesel synthesis [1]. In addition to the use of inexpensive feedstocks, the process from trioses presents the advantage of not being equilibrium-limited.

Years ago Hayashi et al. [9] described the use of alcohol solutions of tin chlorides for the homogeneously catalyzed alkyl lactate synthesis process from trioses, whereas zeolites [10–13] and mixed oxides [14] were postulated as catalysts for the heterogeneous process. More recently, the benefits of using Sn-containing solids such as mesoporous materials (MCM-41 [1,15], SBA-15 [16]), clays [17] and zeolites (MFI [18], BEA [19–23], USY [24]) have been debated in the literature. Processes using Sn-modified materials such as MCM-41 or BEA zeolite produce alkyl lactates in high productivity. However, their industrial implementation may be limited not only by the cost and long synthesis time of these solids but also by the large solid quantities needed for the scaling up of a commodity production.

* Corresponding author.
E-mail address: dicosimo@fiq.unl.edu.ar (J.I. Di Cosimo).

http://dx.doi.org/10.1016/j.cattod.2016.10.002
0920-5861/

In a previous work [25] we reported the synthesis of ethyl lactate from DHA and ethanol on alumina-supported Sn catalysts prepared by impregnation. We showed that on these materials moderate ethyl lactate yields (≈70%) can be obtained at mild conditions giving productivities that depend on the experimental conditions (≥500 g EL/kg cat h) and are comparable to those of other catalytic solids reported in the literature. We focused there on the role played by tin species on the generation of surface acid sites and on the participation of Sn species in the kinetically relevant reaction steps.

In this work we continue our investigations on the ethyl lactate synthesis from DHA and ethanol with emphasis on the reaction kinetics. A series of Sn-alumina oxides containing different Sn contents (1–8 wt.% Sn) were prepared and characterized by several techniques. We investigated the effect of Sn loading and reaction temperature on the reaction kinetics and ethyl lactate yield and postulated a pseudohomogeneous mechanism that well describes the complex reaction system. Kinetic parameters were calculated and their dependence on the catalyst acid properties was elucidated.

2. Experimental

2.1. Catalyst synthesis

Alumina-supported tin catalysts with different Sn content were prepared by incipient wetness impregnation of commercial γ-Al_2O_3 (Cyanamid Ketjen CK 300) with aqueous solutions of $SnCl_4{\cdot}5H_2O$ (Aldrich, 98%). Catalysts were denoted as ZSnAl, where Z is the Sn content expressed in wt.% (Z = 1.4, 4.2, 6.9 and 7.6 wt.% Sn). After impregnation, the solids were thermally treated overnight (18 h) in flowing air at 573 K. The alumina support was treated at 773 K in flowing air for 3 h to remove adsorbed water before the impregnation procedure.

2.2. Catalyst characterization

BET surface areas (*SA*) were measured by N_2 physisorption at 77 K using an Autosorb Quantachrome 1-C sorptometer. The chemical content of Sn in the calcined ZSnAl catalysts was analyzed by inductively coupled plasma (ICP-OES); the catalyst structural properties were determined by X-Ray Diffraction (XRD) between 20° and 80° using a Shimadzu XD-D1 instrument with nickel filtered Cu Kα radiations.

UV-vis-DRS experiments were carried out using a Perkin Elmer Lambda 40 spectrophotometer equipped with a diffuse reflectance chamber and integrating sphere (Labsphere RSA-PE-20) coated internally with polytetrafluoroethylene (PTFE). Prior to each experiment, samples were compacted in a sample holder to obtain a sample thickness of ≈2 mm. Spectra were recorded at room temperature in reflectance mode (*R*) between 200 and 800 nm. More details are given elsewhere [25]. The signal was converted to the Kubelka-Munk function: $F(R_\infty) = (1 - R_\infty)^2/2R_\infty = KC$, where *K* is a constant including the sample scattering coefficient and absorptivity, and *C* is the analyte concentration. The Kubelka-Munk function $F(R_\infty)$ was used to determine the band gap energy (*Eg*) from the plots of $[F(R_\infty) \times (h\nu)]^2$ vs $h\nu$. The *Eg* values were obtained by extrapolation of the linear part of the plots to the *X*-axis [26].

The total acid site number (n_a, μmol/g) was determined by TPD of NH_3. Samples were thermally treated in He 573 K to remove moisture and then exposed to a 1.01% NH_3/He flow at 373 K during 30 min to enable surface saturation. Weakly adsorbed NH_3 was removed by flushing with He. A ramp rate of 10 K/min was used to increase the temperature from 373 K to 593 K; the final temperature was kept constant for 1 h. NH_3 concentration in the reactor effluent was monitored by a mass spectrometer (MS) detector in a Baltzers Omnistar unit.

The chemical nature of the acid sites present on the catalyst surface was determined by Infrared Spectroscopy (IR) of pyridine adsorbed at room temperature and evacuated at increasing temperatures. Details are given elsewhere [25]. The number of Lewis acid sites (n_L, μmol/g) was estimated based on the Lambert-Beer equation: $n_L = \frac{LA}{\varepsilon_L \rho}$ where *LA* (Lewis area in cm^{-1}) stands for the integrated absorption of the band at 1450 cm^{-1} corresponding to pyridine coordinated to Lewis acid sites, and ε_L is the molar extinction coefficient taken as 0.64 cm/μmol [27,28] and ρ is the areal density of the catalyst wafer.

2.3. Catalytic testing

The liquid-phase reaction of dihydroxyacetone, DHA (Aldrich, 97%) with ethanol (Merck, 99.8%) was carried out in a batch PARR reactor. A solution (65 mL) of DHA in ethanol with ethanol/DHA = 43 (molar ratio) was loaded in the reactor at 343–373 K. The catalyst/DHA weight ratio was varied in the range of 21–43%. Catalysts were sieved and the 0.177–0.5 mm fraction was retained. Catalysts were thermally treated ex-situ in air flow at 573 K before the catalytic test. After introducing the reactant mixture the reactor was sealed and flushed with N_2 and then the mixture was heated up to the reaction temperature under stirring (400 rpm) to insure perfect mixing conditions. The catalyst powder was added to the reaction mixture to start the reaction. During the experiments 13–14 samples (≈0.5 mL) were withdrawn from the reactor. Part of the sample extracted (0.15 mL) was mixed with a solution of the standard (*n*-octanol) in ethanol (0.081 mol/L) and analyzed. The rest was reinjected in the reactor. Quantification of reaction products was carried out after proper product identification using a Thermo Scientific Trace 1300 gas chromatograph (GC) with a Thermo Scientific TR-5MS capillary column coupled to a Thermo Scientific ISQ QD MS unit. Main reaction products were glyceraldehyde (GLA), pyruvic aldehyde (PA), ethyl lactate (EL), pyruvic aldehyde hemiacetal (PAHA) and pyruvic aldehyde diethyl acetal (PADA). Minor products include glyceraldehyde diethyl acetal (GLADA). To calculate response factors, solutions containing weighted amounts of the different reactants and products and the standard (*n*-octanol, BDH, 99%) were injected in the GC. All reagents were analytical grade.

Yields (Y_j, mol of product *j*/mol of DHA at $t = 0$) were calculated as $Y_j = S_j\, X_{DHA}$, where X_{DHA} is the conversion of DHA and S_j is the selectivity of product *j* (S_j, mol of product *j*/mol of DHA reacted). Selectivity was calculated as $S_j = C_j/\Sigma C_j$, where C_j is the concentration of product *j*.

The initial DHA conversion rate (r^0_{DHA}, mmol/h g cat) was calculated from the initial slope of the X_{DHA} vs. time curve after multiplication by n^0_{DHA}/W, where n^0_{DHA} is the number of moles of dihydroxyacetone in the reactor at $t = 0$ and *W* is the catalyst load.

2.4. Kinetic modeling, data fitting and statistical analysis

A kinetic study was carried out using a pseudohomogeneous model. The differential equations were solved numerically using the Microsoft Excel Solver software and the Euler method. The relative molar concentrations of all the species over the course of reaction were calculated and compared with the experimental values. Thus, the kinetic parameters were estimated by minimizing the sum of the squared errors (*SSE*) [29] between the experimental data and the data predicted by the model as:

$$SSE = \sum_{all\ data\ samples} \left(C^*_{j\,calc} - C^*_{j\,obs}\right)^2 \quad (1)$$

where C^0_{DHA} is the initial DHA concentration in the reactor expressed in mol DHA/m^3, C^*_j is the relative concentration of compound j (C_j/C^0_{DHA}); $C^*_{j\,calc}$ is the value calculated by applying the model, which is compared with the experimental value ($C^*_{j\,obs}$). The discrimination between models was carried out using the model selection criterion (*MSC*) [30], according to Eq. (2):

$$MSC = \ln\left[\frac{\Sigma\left(C^*_{j\,obs} - \bar{C}^*_{j\,obs}\right)^2}{\Sigma\left(C^*_{j\,obs} - C^*_{j\,calc}\right)^2}\right] - \frac{2p}{m} \quad (2)$$

where $\bar{C}^*_{j\,obs}$ is the mean of measured values, p is the number of parameters; m is the number of experimental observations. The *MSC* parameter is used to compare different models and results independent of the magnitude (scaling) of the data. When comparing different models, the larger the *MSC* value, the better the fit and the more appropriate the model for interpreting the data. The global significance of the regression was evaluated using the *F*-test according to Eq. (3) [31]:

$$F_{calc} = \frac{\dfrac{\sum_{all\ data}\left(C^*_{j\,calc}\right)^2}{\dfrac{samples}{p}}}{\dfrac{\sum_{all\ data}\left(C^*_{j\,calc} - C^*_{j\,obs}\right)^2}{\dfrac{samples}{m-p}}} > F_{tab}\,(\mathrm{p,\ m-p,\ 95\%}) \quad (3)$$

where F_{tab} is obtained from tables [29].

3. Results and discussion

3.1. Catalyst characterization

The ZSnAl catalysts prepared by incipient wetness impregnation of commercial γ-Al_2O_3 followed by calcination in air were analyzed by several techniques in order to study their chemical, structural, textural and acid properties. A detailed discussion of characterization results can be found in a previous work [25]. The most relevant results are summarized in Table 1.

The ZSnAl catalysts presented values of *SA* similar to Al_2O_3. No crystalline Sn species could be detected by XRD analysis thereby indicating that Sn species are well dispersed on the alumina surface forming small domains not detectable by XRD even at loadings close to 8 wt.%. These results were supported by the UV-vis-DRS spectra showing the typical features of SnO_2 nanoparticles [32,33]. Nevertheless, we demonstrated that the band gap energy (*Eg*) of the ZSnAl catalysts measured by UV-vis-DRS (Table 1) gradually decreased as Z increased from 1.4 to 7.6 wt.% Sn. This indicates some degree of agglomeration of Sn species at higher Sn loadings giving rise to larger SnO_2 cluster sizes.

The surface acid properties of the ZSnAl samples were investigated by combining NH_3 TPD and FTIR of pyridine. The total acid site number (n_a, μmol/g) was calculated by integration of the NH_3 TPD traces (not shown) and the data are reported in Table 1. The desorption temperature and the n_a values of the ZSnAl samples were much higher than those of the support, therefore confirming that surface Sn species are responsible for the generation of new and stronger acid sites compared to those of γ-Al_2O_3.

The chemical nature of the surface acid sites present on ZSnAl and γ-Al_2O_3 catalysts was studied by FTIR of pyridine preadsorbed at room temperature and evacuated at increasing temperatures. Alumina is known to be a typical Lewis acid solid and the Lewis acid character of the ZSnAl samples was confirmed by the bands at 1450 and 1618 cm^{-1} assigned to pyridine coordinated on the oxide cations [34]. No band indicative of the presence of Brønsted acid sites (≈1640 and 1550 cm^{-1}) was detected. The number of Lewis acid sites (n_L) was calculated by integration of the band at 1450 cm^{-1} for the ZSnAl samples and alumina (Table 1). A good agreement was found between n_L and the n_a values determined by TPD of NH_3 confirming that the solids only contain Lewis sites. Thus, we assume that the measured number of acid sites (n_a) essentially corresponds to titration of Lewis acid centers provided by Al^{3+} and Sn^{4+} cations.

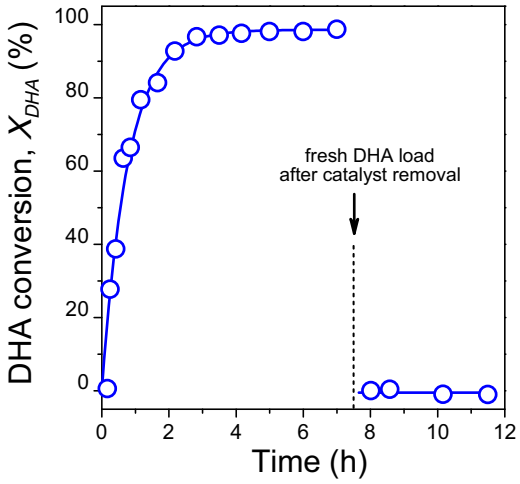

Fig. 1. DHA conversion (X_{DHA}) as a function of reaction time on 6.9SnAl. Catalyst removal at 7 h [353 K; ethanol/DHA = 43 (molar); 1 g of catalyst].

3.2. General features of the ethyl lactate synthesis on ZSnAl catalysts

The ethyl lactate (EL) synthesis was studied in a batch reactor. Previous to the catalytic tests, blank tests were carried with DHA and ethanol at 353 K without any catalyst. Thermal reactions were ruled out since no measurable conversion was found after 7 h under those conditions.

The ZSnAl samples of Table 1 prepared by impregnation of alumina followed by calcination were tested at 353 K for the conversion of DHA and ethanol to EL. Initially, the heterogeneous nature of the synthesis process was confirmed. Fig. 1 shows the experiment carried out with sample 6.9SnAl at 353 K. Total DHA conversion (X_{DHA}) was reached at 7 h. After this, the solid catalyst was removed and a fresh DHA load was added to the reactor. The reaction was continued for 4 more hours at 353 K but no conversion was observed. This confirms the absence of Sn in the liquid phase to continue the reaction and therefore, the contribution of a homogeneously catalyzed reaction can be ruled out.

Prior to any kinetic measurement, the presence of external and internal diffusional limitations was studied. The extent of the external mass transfer resistance was evaluated by calculating the Mears number (ω) [35]:

$$\omega = \frac{r^0_{DHA}\rho_p R_p}{k_c C^0_{DHA}} < \frac{0.15}{n} \quad (4)$$

where r^0_{DHA} is the initial DHA conversion rate (30.4 mol/h kg) for the experiment of Fig. 1, ρ_p is the catalyst particle density (1563 kg/m^3), R_p is the average particle radius (1.7×10^{-4} m), k_c is the mass transfer coefficient (0.67 m/h) calculated as $k_c = \frac{ShD_m}{2R_p}$, where D_m (1.25×10^{-5} m^2/h) is the molecular diffusion coefficient calculated from the Wilke-Chang correlation [36], *Sh* is the Sherwood number $\left(Sh = 2 + 0.55Re^{0.5}Sc^{0.33}\right)$, *Re* is the Reynolds number and *Sc*

Table 1
Physicochemical properties of alumina-supported Sn catalysts.

Catalyst	Sn loading, *Z* (wt.%)	Surface area, *SA* (m^2/g)	UV-vis-DRS analysis	Acidic Properties	
			Band gap energy, *Eg* (eV)	n_a[a] (μmol/g)	n_L[b] (μmol/g)
1.4SnAl	1.4	216	4.98	103	101
4.2SnAl	4.2	188	4.93	121	149
6.9SnAl	6.9	184	4.86	165	189
7.6SnAl	7.6	222	4.83	201	193
γ-Al_2O_3	–	230	–	24	86

[a] By TPD of NH_3.
[b] By FTIR of pyridine.

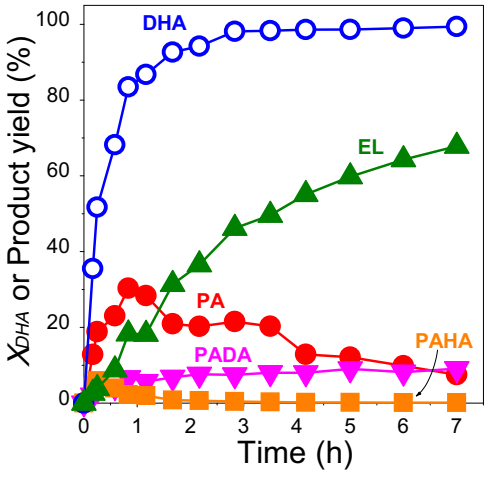

Fig. 2. DHA conversion (X_{DHA}) and product yields as a function of reaction time on 7.6SnAl [353 K; ethanol/DHA = 43 (molar); 1 g of catalyst].

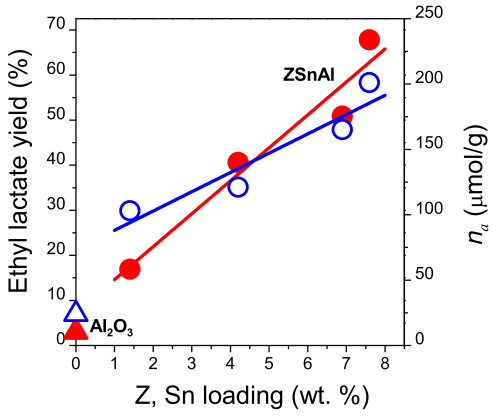

Fig. 3. Ethyl lactate yield (closed symbols) and acid site number (n_a, open symbols) as a function of the Sn loading (Z) for ZSnAl catalysts. Al_2O_3 included as reference. Circles: ZSnAl catalysts; Triangles: γ-Al_2O_3 [353 K; ethanol/DHA = 43 (molar); 1 g of catalyst; 7 h].

is the Schmidt number [37–40]. C^0_{DHA} is the initial DHA concentration (4×10^2 mol/m^3) and *n* is the reaction order taken as 1. Thus, a ω value of 0.03 was calculated thereby confirming the absence of interparticle diffusion limitations. To verify the absence of intraparticle mass transfer limitations, the Weisz-Prater criterion [41] for a first order reaction and spherical catalyst particles was used:

$$\Phi = \frac{r^0_{DHA}\rho_p R^2_p}{D_{eff} C^0_{DHA}} < 1 \quad (5)$$

where Φ is the dimensionless Weisz-Prater modulus, D_{eff} is the effective diffusion coefficient (6.4×10^{-6} m^2/h) calculated using a particle porosity of 0.51. A value of 0.54 was calculated for Φ, which corresponds to a Thiele modulus of 0.36 and an effectiveness factor of 0.96. This result confirms the absence of pore diffusion limitations. Then, no diffusional limitations seem to be present under typical reaction conditions and the reaction takes place under kinetic control.

Fig. 2 shows the time evolution of the X_{DHA} and of the major product yields obtained at 353 K on sample 7.6SnAl. Total DHA conversion and a 68% lactate yield could be obtained at the end of the 7h-run using reaction conditions similar to those previously reported in the literature for other catalysts [1,14,15,23]. Main products were ethyl lactate (EL), pyruvic aldehyde (PA), pyruvic aldehyde diethyl acetal (PADA) and pyruvic aldehyde hemiacetal (PAHA). The shape of the curves clearly indicates that PA and PAHA are reaction intermediates whereas PADA and EL are final products.

Based on the results of Fig. 2, the reaction pathways conducting to EL and other products are postulated in Scheme 1. DHA is initially isomerized to glyceraldehyde (GLA) [42], step 1, but under our reaction conditions the equilibrium of step 1 is expected to be shifted toward DHA [13,43]. Both trioses give similar product distribution when react with an alcohol [10,11]. Thus, in our calculations X_{DHA} stands for the overall conversion of both trioses. Step 2 is the triose (DHA and GLA) dehydration to PA. From PA the reaction pathway might proceed toward the desired ethyl lactate product by re-arrangement with incorporation of an alcohol molecule step 3, or toward PAHA (step 4) and PADA (step 5) by addition of an alcohol molecule in each of these reaction steps. Step 6 is the isomerization of PAHA to EL.

Due to the complex nature of the DHA conversion on ZSnAl, in the following sections we will focus on the optimization of the EL formation and on the competing pathways leading to the final products EL and PADA.

3.3. *Effect of the experimental conditions*

The effect of varying experimental parameters such as Sn loading, catalyst load and reaction temperature on the activity and product distribution was investigated.

Fig. 3 shows the EL yields obtained at 353 K after the 7h-run on the ZSnAl catalysts with different Sn loadings (Z = 1.4, 4.2, 6.9 and 7.6 wt.% Sn). Clearly, the EL yield (closed circles) increases linearly with Z in a similar fashion to n_a (open circles). It seems that the bimolecular nature of the reactions involved in EL formation requires not only a high number of Sn species available for reaction but also the close proximity of those species to allow the vicinal chemisorption of the different reaction intermediates. Furthermore, the EL yields are much higher than on γ-Al_2O_3 (closed triangle). As we stated above, alumina presents in general, poor acidic properties and in particular, a low value of n_a (open triangle). Although alumina is a Lewis acid, it seems that the Al^{3+} cations are not acidic enough to transform DHA into EL to a significant extent. Thus, on the Sn-containing samples, highly dispersed Sn^{4+} species with Lewis acid properties are responsible for promoting the EL formation.

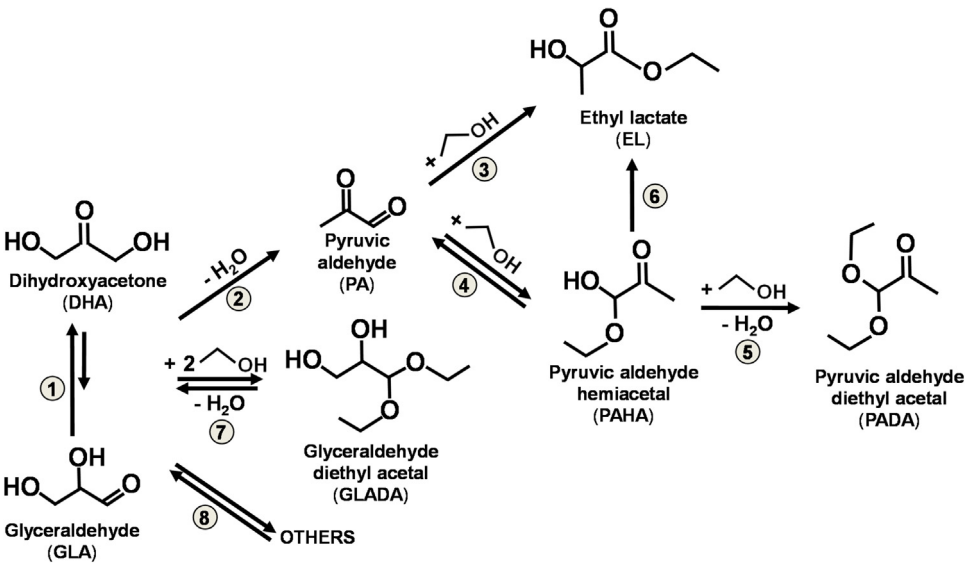

Scheme 1. Reaction steps for the synthesis of ethyl lactate and other oxygenates from DHA and ethanol on Sn-promoted alumina catalysts.

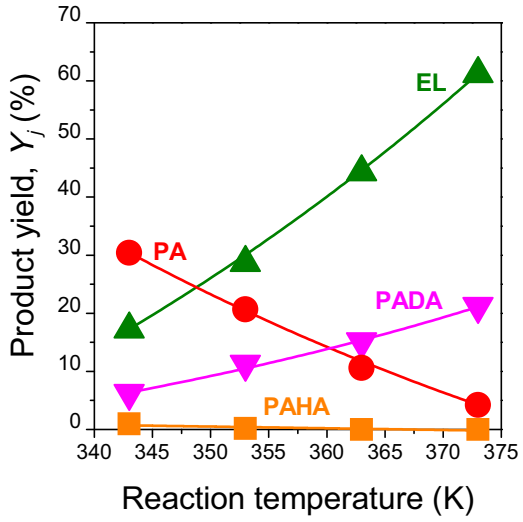

Fig. 4. Yields to main products as a function of the reaction temperature on 7.6SnAl [ethanol/DHA = 43 (molar); 0.5 g of catalyst; 7 h].

The effect of the reaction temperature on the yield to EL and other products was investigated with sample 7.6SnAl. Fig. 4 presents the results obtained after the 7h-run at 343, 353, 363 and 373 K showing that the yield toward both end products, EL and PADA, increase with temperature at the expense of the intermediate PA in the temperature range under study. On the other hand, the contribution of PAHA, the intermediate from which PADA and EL are formed, is irrelevant at any temperature.

The time evolution of the main products can be compared at the different temperatures in Fig. 5. It is noticeable the decrease of the maximum PA yield and its shift toward lower times as the temperature increases.

The time evolution of X_{DHA} for the different reaction temperatures is also plotted in Fig. 5; with increasing the temperature, a gradual increase of the final X_{DHA} from 88% to 99% is observed.

The experiments of Fig. 3 and 4 were carried out at a different catalyst load. Thus, on sample 7.6SnAl at the end of the 7h-run at 353 K the EL yield (Y_{EL}) resulting from the experiment with 0.5 g (Fig. 4) was 29% whereas that obtained with 1 g (Fig. 3) was 68%.

All these results indicate that the reaction is not equilibrium-limited and that the final X_{DHA} and Y_{EL} depend on the amount of catalyst used, the catalyst Sn content and the reaction temperature. Furthermore, Y_{EL} can be improved by implementing the reaction at the highest values of these experimental variables.

3.4. Kinetics of the DHA conversion on ZSnAl catalysts

A kinetic model was postulated following the reaction sequence depicted in Scheme 1. Seven catalytic runs comprising the experiments varying the Sn loading and the reaction temperature were modeled with a total of ≈750 data points. Our goal was to calculate the kinetic constants (k_i) and to analyze their dependence on the temperature and acid properties.

In a previous work [25] we discussed the participation of Brønsted and Lewis acid sites on ethyl lactate and other oxygenate formation and postulated a mechanism for EL and PADA formation on ZSnAl catalysts. It is generally accepted that PA formation is promoted by mild Brønsted acid sites but some authors claim the participation of Lewis acid sites [1,13]. From PA, formation of the terminal products EL and PADA involves sites with different acid nature; whereas the former occurs on Lewis sites the latter takes place on Brønsted sites.

Furthermore, we discussed that the two parallel pathways (step 3 or step 6 of Scheme 1) leading to EL are promoted by Lewis acid sites. Scheme 2 summarizes the surface reactions for these two steps. Step 3 is in fact a reaction sequence in which PA and ethanol are first activated on the surface followed by the nucleophilic addition of the ethoxide intermediate to the adsorbed PA molecule and formation of an anionic cyclic intermediate. Then, ethyl lactate is released after intramolecular rearrangement with a 1,2-hydride shift. Step 6, on the other hand, is the isomerization of PAHA and involves a bidentate PAHA coordination on a Sn atom and the O—H bond breaking, followed by formation of an intermediate similar to that of the pathway from PA, and intramolecular rearrangement with a shift of the hydride. Thus, another objective of the kinetic study was to identify which of the two pathways toward EL formation predominates on ZSnAl catalysts.

The kinetic study was carried out using a pseudohomogeneous model to interpret the catalytic data. Firstly, we assumed that the main products of the triose (DHA and GLA) conversion were PA, EL,

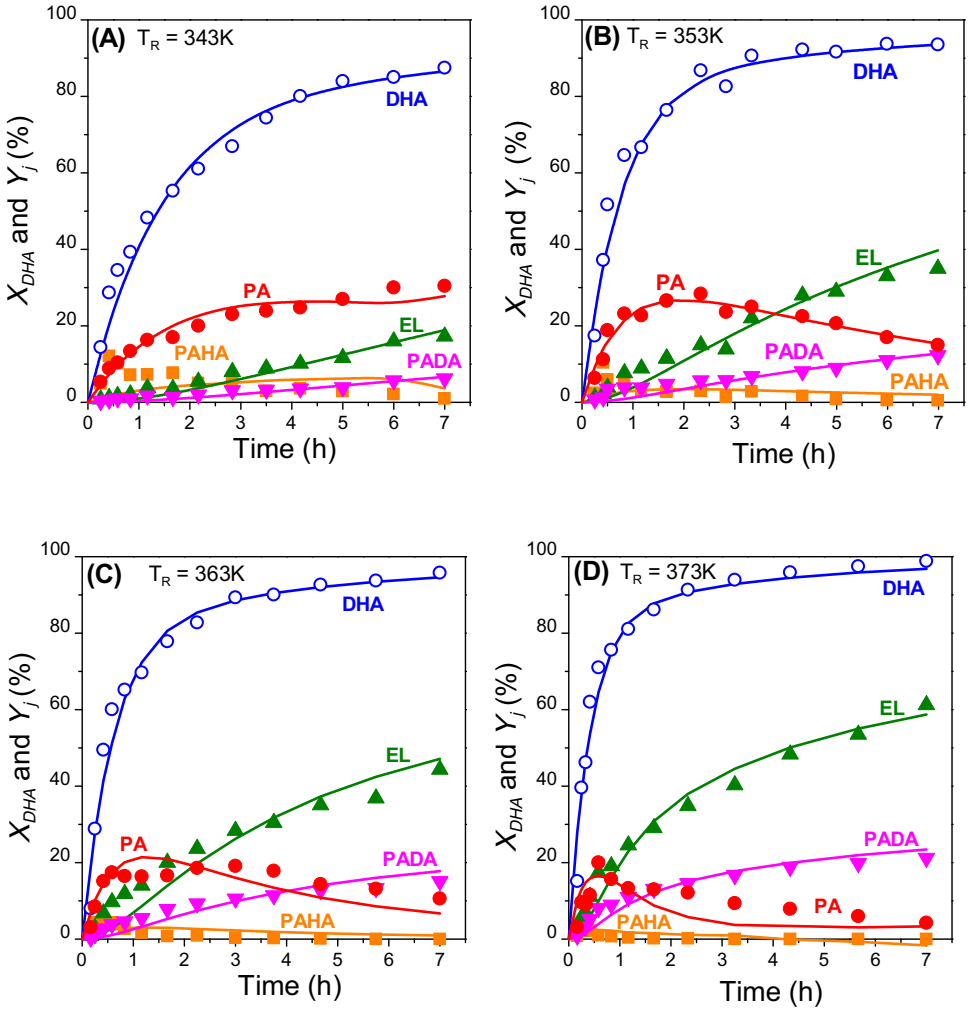

Fig. 5. DHA conversion and product yields as a function of time on 7.6SnAl at different reaction temperatures. (A) 343 K; (B) 353 K; (C) 363 K; (D) 373 K. Symbols: experimental data; Lines: model [ethanol/DHA = 43 (molar); 0.5 g of catalyst].

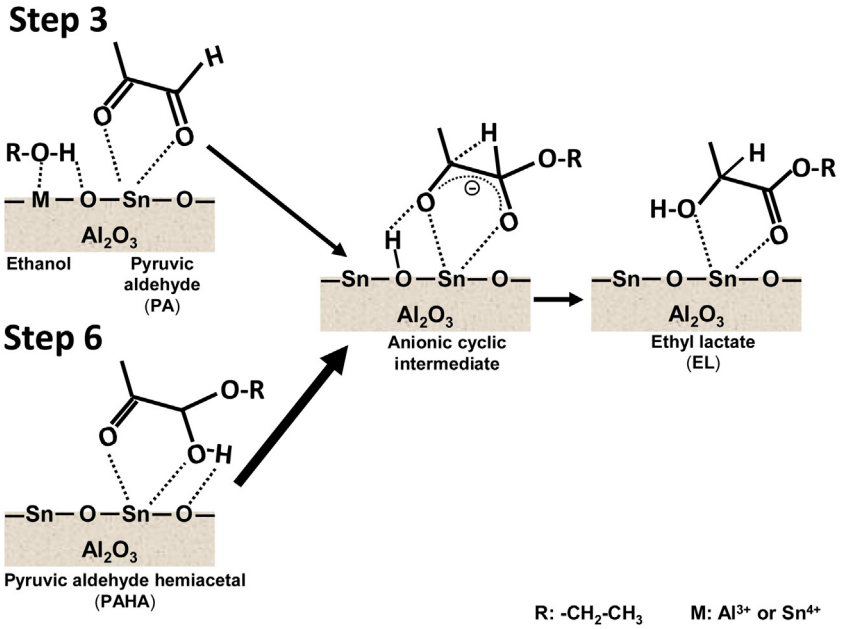

Scheme 2. Simplified Sn-promoted formation of EL from PA (step 3) and from PAHA (step 6). Step numbers as in Scheme 1.

PAHA, PADA and GLADA; minor products present in low concentration were grouped as OTHERS.

First order rate equations respect to DHA and products were used. The reaction order respect to ethanol was taken as zero since ethanol is in excess in the reaction mixture and therefore its concentration (C^0_{EtOH}) remains constant during the typical 7h-run.

Initially, the modeling was carried out using a large number of parameters because all the steps of Scheme 1 were considered as reversible reactions. As a result of those assumptions, small values of the kinetic constants for the reverse reactions of steps 2, 3, 5 and 6 were obtained. Thus, calculations were repeated assuming that these kinetic constants were equal to zero whereas the steps forming PAHA, GLADA and OTHERS (steps 4, 7 and 8, respectively, in Scheme 1) were considered as reversible transformations.

In a further step of the modeling process, we attempted to elucidate which of the two Lewis acid promoted-pathways to EL formation depicted in Scheme 2, either the direct synthesis from PA (step 3) or from PAHA (step 6) was kinetically favored under our reaction conditions. Thus, two cases were postulated in which k_3 or k_6 were taken as zero and the kinetic and statistical parameters obtained in both cases were compared. The results obtained by modeling the experimental data with these two different restrictions show that the best fit was obtained with $k_3 = 0$. In addition, the *SSE* and *MSC* values were similar for both models (≈3) but the confidence intervals (*CI*) obtained with calculation considering $k_6 = 0$ took values that could make negative some of the k_i parameters. On the other hand, for the calculations with $k_3 = 0$ the *CI* values were statistically consistent. Therefore, the calculation results that will be discussed below were obtained assuming $k_3 = 0$.

Then, it was concluded that formation of EL mainly proceeds through the PAHA intermediate in agreement with the results of Li et al. on Sn-MCM-41 [15] and of van der Graaff et al. on Sn-BEA [23]. Thus, the thickness of the arrow lines in Scheme 2 indicates the relative importance of the two mechanisms toward EL on ZSnAl catalysts, emphasizing that EL mainly arises from PAHA and to a lesser extent directly from PA.

With the assumptions discussed above, the mass balances for the different components of the reaction mixture (before reparametrization of C_j to dimensionless relative concentrations C^*_j) are given by the differential Eqs. (6)–(12):

$$\frac{n^0_{DHA}}{W}\frac{dC^*_{DHA}}{dt} = -r_2 - r_7 - r_8 \quad (6)$$

$$\frac{n^0_{DHA}}{W}\frac{dC^*_{PA}}{dt} = r_2 - r_4 \quad (7)$$

$$\frac{n^0_{DHA}}{W}\frac{dC^*_{EL}}{dt} = r_6 \quad (8)$$

$$\frac{n^0_{DHA}}{W}\frac{dC^*_{PAHA}}{dt} = r_4 - r_5 - r_6 \quad (9)$$

$$\frac{n^0_{DHA}}{W}\frac{dC^*_{PADA}}{dt} = r_5 \quad (10)$$

$$\frac{n^0_{DHA}}{W}\frac{dC^*_{GLADA}}{dt} = r_7 \quad (11)$$

$$\frac{n^0_{DHA}}{W}\frac{dC^*_{OTHERS}}{dt} = r_8 \quad (12)$$

where r_2, r_4, r_5, r_6, r_7 and r_8 stand for the reaction rates of steps 2, 4, 5, 6, 7 and 8, respectively, according to Scheme 1 and expressed in mol/h kg. The kinetic rate expressions for the proposed model are given in Eqs. (13)–(18):

$$r_2 = k_2 C_{DHA} \quad (13)$$

$$r_4 = k^*_4 C_{PA} - k_{-4} C_{PAHA} \quad (14)$$

Table 2
Activation energies (E_a) resulting from modeling the results of Fig. 5.

Reaction step	E_a (Kcal/mol)
2	10.5
4	0.0
−4	0.0
5	24.2
6	22.9
7	16.6
−7	7.4
8	6.6
−8	10.3

$$r_5 = k^*_5 C_{PAHA} \quad (15)$$

$$r_6 = k_6 C_{PAHA} \quad (16)$$

$$r_7 = k^*_7 C_{DHA} - k_{-7} C_{GLADA} \quad (17)$$

$$r_8 = k_8 C_{DHA} - k_{-8} C_{OTHERS} \quad (18)$$

where k_i and k_{-i} represent the kinetic constant of the forward and the reverse reaction, respectively, and k^*_4, k^*_5 and k^*_7 are parameters involving the kinetic constant and the ethanol concentration:

$$k^*_4 = C^0_{EtOH} k_4 \quad (19)$$

$$k^*_5 = C^0_{EtOH} k_5 \quad (20)$$

$$k^*_7 = C^0_{EtOH} k_7 \quad (21)$$

The postulated kinetic model was contrasted with the experimental data of Fig. 5. Eqs (6)–(18) were numerically integrated via a Runge-Kutta method and the nine kinetic parameters (k_i) were calculated. The lines in Fig. 5 indicate that the experimental data obtained at different reaction temperatures with sample 7.6SnAl are well fitted by the postulated model.

With the k_i values predicted by the model the corresponding activation energies (E_a) were calculated using the Arrhenius equation. Table 2 summarizes the results. Clearly, the highest E_a values were obtained for step 6 leading to EL and the competing formation of PADA through step 5. Thus, these are the kinetically relevant steps and show similar E_a values. On the other hand, the reversible formation of the intermediate PAHA is insensitive to the reaction temperature.

In a similar fashion, Eqs. (6)–(18) were numerically integrated for the experiments at 353 K carried out with ZSnAl catalysts containing different Sn contents. A set of nine kinetic parameters (k_i) were obtained for each catalyst.

The most relevant kinetic parameters k_5 and k_6 are plotted in Fig. 6A as a function of the number of acid sites (n_a) of each catalyst. As discussed in Section 3.1, n_a essentially reflects the number of Lewis acid sites because no band indicative of the presence of Brønsted acid sites was detected by FTIR of pyridine. In addition, as shown in Fig. 3, n_a increases linearly with the catalyst Sn content. Thus, the fact that the kinetic constant of the main route to EL formation (k_6) is strongly dependent on the Lewis acid site content confirms the participation of Sn species in the isomerization of PAHA, as postulated in Scheme 2. On the other hand, k_5, the kinetic constant for PADA formation, shows almost no dependence on n_a. This result seems to suggest that another site promotes step 5. As discussed above, PADA can be obtained in high yields on Brønsted acid solids. Isolated OH groups remaining on the surface of the Sn-promoted oxides after calcination might behave as Brønsted acid sites that promote step 5; these sites are fairly weak since they do not protonate pyridine [25]. Another possibility is the generation of weak OH groups during reaction due to water formation through step 2. However, the amount of the OH species generated in situ should be low since ethanol competes favorably with water for the adsorption sites and probably displaces it from the surface [44].

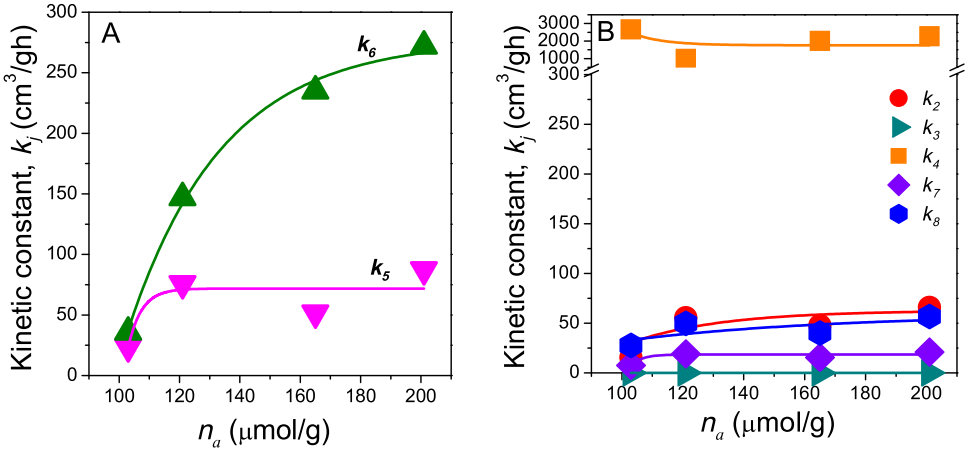

Fig. 6. Kinetic constants as a function of the acid site number (n_a) of ZSnAl catalysts. (A) for steps 5 (k_5) and 6 (k_6); (B) for steps 2 (k_2), 3 (k_3), 4 (k_4), 7 (k_7) and 8 (k_8). Step numbers as in Scheme 1 [353 K; ethanol/DHA = 43 (molar)].

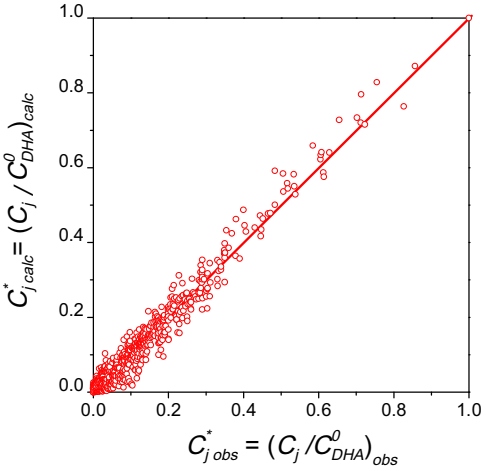

Fig. 7. Parity plot of the experimental ($C^*_{j\,obs} = \left(C_j/C^0_{DHA}\right)_{obs}$) and predicted ($C^*_{j\,calc} = \left(C_j/C^0_{DHA}\right)_{calc}$) relative concentrations of DHA and products.

Besides k_5 and k_6, the other kinetic constants for direct reaction steps are presented in Fig. 6B. The largest k_i value was calculated for PAHA formation (k_4) whereas the other kinetic constants were comparable to k_5.

A parity plot of the experimental ($C^*_{j\,obs} = \left(C_j/C^0_{DHA}\right)_{obs}$) and calculated ($C^*_{j\,calc} = \left(C_j/C^0_{DHA}\right)_{calc}$). relative concentrations of the reaction mixture components is given in Fig. 7. Although the modeling involved 750 experimental observations and was carried out with four catalysts and at four different reaction conditions, Fig. 7 shows that the pseudohomogeneous model well represents the experimental data. The *SSE* parameter calculated with Eq. (1) was in all the regressions in the range of 0.06–0.09, whereas the value of the correlation coefficient (R^2) was always higher than 0.98. Moreover, from Eq. (3) a value of $F_{calc} = 754$ was obtained whereas the corresponding F_{tab} was ≈1.3, indicating that the model is suitable for predicting the DHA conversion reactions.

4. Conclusions

Upgrading of triose sugars into valuable chemicals can be performed on alumina-supported Sn catalysts easily prepared by impregnation. In particular, ethyl lactate yields of up to 68% can be obtained from dihydroxyacetone and ethanol on a 7.6 wt.%Sn/Al_2O_3 catalyst at 353 K.

On the Sn-alumina oxides both, the number of Lewis acid sites and the ethyl lactate yield increase linearly with the catalyst Sn loading. The increase of the reaction temperature favors ethyl lactate formation at the expense of the intermediate pyruvic aldehyde.

The reaction proceeds through a complex reaction network with formation of ethyl lactate and other intermediate and final products. The reaction kinetics can be well described by a pseudohomogeneous mechanism and first order rate expressions. The kinetic parameter associated to ethyl lactate formation increases with the number of Lewis acid sites confirming that surface Sn species are responsible for the catalytic activity of these materials.

Acknowledgements

Authors thank the Agencia Nacional de Promoción Científica y Tecnológica (ANPCyT), Argentina (grant PICT 1888/10), CONICET, Argentina (grant PIP 11220090100203/10) and Universidad Nacional del Litoral, Santa Fe, Argentina (grant CAID PI 64-103/11) for financial support of this work.

References

[1] F. de Clippel, M. Dusselier, R. Van Rompaey, P. Vanelderen, J. Dijkmans, E. Makshina, L. Giebeler, S. Oswald, G.V. Baron, J.F.M. Denayer, P.P. Pescarmona, P.A. Jacobs, B.F. Sels, J. Am. Chem. Soc. 134 (2012) 10089–10101.
[2] T.N.B. Kaimal, P. Vijayalakshmi, B. Ramalinga, A. A. Laxmi, US Patent N° 6342626 (2002).
[3] C.S.M. Pereira, V.M.T.M. Silva, A.E. Rodrigues, Green Chem. 13 (2011) 2658–2671.
[4] S. Aparicio, R. Alcalde, J. Phys. Chem. B 113 (2009) 14257–14269.
[5] A. Corma, S. Iborra, A. Velty, Chem. Rev. 107 (2007) 2411–2502.
[6] A. Engin, H. Haluk, K. Gurkan, Green Chem. 5 (2003) 460–466.
[7] M.T. Sanz, R. Murga, S. Beltrán, J.L. Cabezas, J. Coca, Ind. Eng. Chem. Res. 41 (2002) 512–517.
[8] C.L. Bianchi, P. Canton, N. Dimitratos, F. Porta, L. Prati, Catal. Today 102–103 (2005) 203–212.
[9] Y. Hayashi, Y. Sasaki, Chem. Commun. (2005) 2716–2718.
[10] P.P. Pescarmona, K.P.F. Janssen, C. Delaet, C. Stroobants, K. Houthoofd, A. Philippaerts, C. De Jonghe, J.S. Paul, P.A. Jacobs, B.F. Sels, Green Chem. 12 (2010) 1083–1089.
[11] R.M. West, M.S. Holm, S. Saravanamurugan, J. Xiong, Z. Beversdorf, E. Taarning, C.H. Christensen, J. Catal. 269 (2010) 122–130.
[12] K.P.F. Janssen, J.S. Paul, B.F. Sels, P.A. Jacobs, Stud. Surf. Sci. Catal. 70 (B (2007) 1222–1227.
[13] P.Y. Dapsens, B.T. Kusema, C. Mondelli, J. Pérez-Ramírez, J. Mol. Catal. A: Chem. 388–389 (2014) 141–147.
[14] A.M. Mylin, S.I. Levytska, M.E. Sharanda, V.V. Brei, Catal. Commun. 47 (2014) 36–39.

[15] L. Li, C. Stroobants, K. Lin, P.A. Jacobs, B.F. Sels, P.P. Pescarmona, Green Chem. 13 (2011) 1175–1181.
[16] C.M. Osmundsen, M.S. Holm, S.D, E. Taarning, Proc. R. Soc. A (2012) 1–17.
[17] J. Wang, Y. Masui, M. Onaka, Appl. Catal. B: Environ. 107 (2011) 135–139.
[18] H.J. Cho, P. Dornath, W. Fan, ACS Catal. 4 (2014) 2029–2037.
[19] J. Dijkmans, M. Dusselier, D. Gabriels, K. Houthoofd, P.C.M.M. Magusin, S. Huang, Y. Pontikes, M. Trekels, A. Vantomme, L. Giebeler, S. Oswald, B.F. Sels, ACS Catal. 5 (2015) 928–940.
[20] C. Hammond, S. Conrad, I. Hermans, Angew. Chem. Int. Ed. 51 (2012) 11736–11739.
[21] E. Taarning, S. Saravanamurugan, M.S. Holm, J. Xiong, R.M. West, C.H. Christensen, ChemSusChem 2 (2009) 625–627.
[22] S. Tolborg, A. Katerinopoulou, D.D. Falcone, I. Sádaba, C.M. Osmundsen, R.J. Davis, E. Taarning, P. Fristrup, M.S. Holm, J. Mater. Chem. A 2 (2014) 20252–20262.
[23] W.N.P. van der Graaff, G. Li, B. Mezari, E.A. Pidko, E.J.M. Hensen, ChemCatChem 7 (7) (2015) 1152–1160.
[24] X. Yang, L. Wu, Z. Wang, J. Bian, T. Lu, L. Zhou, C. Chen, J. Xu, Catal. Sci. Technol. 6 (2016) 1757–1763.
[25] E. Pighin, V.K. Díez, J.I. Di Cosimo, Appl. Catal, A. General, Appl. Catal. A: Gen. 517 (2016) 151–160.
[26] S. Roy, K. Bakhmutsky, E. Mahmoud, R.F. Lobo, R.J. Gorte, ACS Catal. 3 (2013) 573–580.
[27] E. Selli, L. Forni, Microporous Mesoporous Mater. 31 (1999) 129–140.
[28] M. Tamura, K. Shimizu, A. Satsuma, Appl. Catal. A: Gen. 433–434 (2012) 135–145.
[29] R.E. Walpole, R.H. Myers, S.L. Myers, K.E. Ye, Probability & Statistics for Engineers & Scientists, 8th Edition, Pearson Prentice Hall, Upper Saddle River, 2007, ISBN 0-13-204767-5.
[30] S. Armenise, E. García-Bordeje, J.L. Valverde, E. Romeo, A. Monzón, Phys. Chem. Chem. Phys. 15 (2013) 12104–12117.
[31] E. Van de Steene, J. De Clercq, J.W. Thybaut, J. Mol. Catal. A: Chem. 359 (2012) 57–68.
[32] G. Pang, S. Chen, Y. Koltypin, A. Zaban, S. Feng, A. Gedanken, Nano Lett. 1 (12) (2001) 723–726.
[33] H. Deng, J.M. Hossenlopp, J. Phys. Chem. B 109 (2005) 66–73.
[34] M.I. Zaki, M.A. Hasan, F.A. Al-Sagheer, L. Pasupulety, Colloids Surf. A: Phys. Eng. Aspects 190 (2001) 261–274.
[35] D.E. Mears, Ind. Eng. Chem. Proc. Des. Dev. 10 (4) (1971) 438–447.
[36] C.R. Wilke, P. Chang, AIChE J. (1955) 264–270.
[37] T. Dossin, Kinetics and Reactor Modelling of MgO-Catalysed Transesterification for Sustainable Development, Universiteit Gent, 2006, ISBN: 90-8578-079-9.
[38] Dortmund data bank: http://www.ddbst.com.
[39] J.R. Couper, W.R. Penney, J.R. Fair, S.M. Walas, Chemical Process Equipment: Selection and Design, second edition, Gulf Professional Publishing (GPP), 2005, pp. 287–292, ISBN: 978-0-7506-7510-9.
[40] H.S. Fogler, Elements of Chemical Reaction Engineering, 3rd ed., Prentice Hall, 1999.
[41] P.B. Weisz, C.D. Prater, Adv. Catal. 6 (1954) 143–196.
[42] V.A. Yaylayan, S. Harty-Majors, A.A. Ismail, Carbohydr. Res. 318 (1999) 20–25.
[43] R.S. Assary, L.A. Curtiss, J. Phys. Chem. A 115 (2011) 8754–8760.
[44] G. Busca, Catal. Today 226 (2014) 2–13.